

Highly crystalline MoS₂ thin films grown by pulsed laser deposition

Cite as: Appl. Phys. Lett. **106**, 052101 (2015); <https://doi.org/10.1063/1.4907169>

Submitted: 19 November 2014 • Accepted: 20 January 2015 • Published Online: 02 February 2015

 Claudy R. Serrao, Anthony M. Diamond,  Shang-Lin Hsu, et al.



View Online



Export Citation



CrossMark

ARTICLES YOU MAY BE INTERESTED IN

[Growth of centimeter-scale atomically thin MoS₂ films by pulsed laser deposition](#)

APL Materials **3**, 056103 (2015); <https://doi.org/10.1063/1.4921580>

[Emerging photoluminescence from bilayer large-area 2D MoS₂ films grown by pulsed laser deposition on different substrates](#)

Journal of Applied Physics **122**, 015304 (2017); <https://doi.org/10.1063/1.4991490>

[Investigation of the optical properties of MoS₂ thin films using spectroscopic ellipsometry](#)

Applied Physics Letters **104**, 103114 (2014); <https://doi.org/10.1063/1.4868108>



Time to get excited.
Lock-in Amplifiers – from DC to 8.5 GHz

[Find out more](#)

 Zurich Instruments

Highly crystalline MoS₂ thin films grown by pulsed laser deposition

Claudy R. Serrao,¹ Anthony M. Diamond,² Shang-Lin Hsu,² Long You,¹ Sushant Gadgil,¹ James Clarkson,² Carlo Carraro,³ Roya Maboudian,³ Chenming Hu,¹ and Sayeef Salahuddin¹

¹Department of Electrical Engineering and Computer Sciences, University of California, Berkeley, California 94720, USA

²Department of Material Science and Engineering, University of California, Berkeley, California 94720, USA

³Department of Chemical and Biomolecular Engineering, University of California, Berkeley, California 94720, USA

(Received 19 November 2014; accepted 20 January 2015; published online 2 February 2015)

Highly crystalline thin films of MoS₂ were prepared over large area by pulsed laser deposition down to a single monolayer on Al₂O₃ (0001), GaN (0001), and SiC-6H (0001) substrates. X-ray diffraction and selected area electron diffraction studies show that the films are quasi-epitaxial with good out-of-plane texture. In addition, the thin films were observed to be highly crystalline with rocking curve full width half maxima of 0.01°, smooth with a RMS roughness of 0.27 nm, and uniform in thickness based on Raman spectroscopy. From transport measurements, the as-grown films were found to be p-type. © 2015 AIP Publishing LLC. [<http://dx.doi.org/10.1063/1.4907169>]

Two dimensional (2D) materials have garnered great interest in recent years due to their unique electronic, mechanical, and optical properties.^{1,2} 2D materials can be found in nature as bulk solids, formed from the stacking of strongly bonded layers that are held together by weaker van der Waals interaction. This characteristic of the bulk materials has opened the way to experimentally investigate the properties of individual layers through the method of exfoliation.³ One of the materials of great scientific interest has been graphene which exhibits a conical Dirac energy spectrum near the K point, producing charge carriers that can be described as essentially massless Dirac fermions that have important consequences for thermal conductivity and carrier mobility.^{4,5} Though the band-structure of graphene is the source of many interesting properties, there is no gap in the density of states which makes graphene incompatible with applications such as traditional electronic switching devices. By contrast, transition metal dichalcogenides (TMD) that consist of stacked layers of covalently bonded transition metal and group six atoms have large band-gaps as a result of the broken symmetry in the atomic basis set. Field-effect transistor (FET) devices made from TMD materials could potentially provide large on/off ratios (>10⁶) and excellent electrostatic integrity at ultra-scaled dimensions.^{6–8} However, to materialize the promise of these TMD materials, appropriate methods for large area growth must be developed. To that end, extensive efforts have been applied following different approaches such as intercalation assisted exfoliation,^{9–11} micromechanical exfoliation using scotch tape,^{12–15} liquid exfoliation,¹⁶ hydrothermal synthesis,¹⁷ thermolysis of single precursors,^{18,19} chemical vapor deposition,²⁰ vapor solid epitaxy,²¹ and physical vapor deposition.^{22–24} Recently, vapor-solid grown MoS₂ has been shown to have excellent electronic quality.²¹ However, the lateral dimensions of films synthesized by these various methods have mostly been limited to the order of a few hundred microns.

Physical Vapor Deposition methods, particularly Pulsed Laser Deposition (PLD), have been explored less. Recently, there are a couple of reports of MoS₂ growth by PLD.^{25,26}

Late *et al.* deposited films containing dense nanostructures of MoS₂ on W and Si and studied the field emission and photo-response.²⁵ MoS₂ growth mechanism by PLD on metal substrates like Al, Ag, Ni, and Cu have been studied.²⁶ In this paper, we demonstrate that highly crystalline thin films consisting of a few monolayers (ML) of MoS₂ can be synthesized over large areas by pulsed laser deposition.

MoS₂ thin films (1–15 ML) were deposited by pulsed laser deposition. One inch diameter targets were made by cold isostatic pressing of MoS₂ and sulfur powder with varying Mo to S atomic ratios. The powders were obtained from Sigma-Aldrich and used as received. The targets were placed 5 cm away from 5 × 5 mm² substrates of single-side polished Al₂O₃ (0001), GaN (0001), and SiC-6H (0001). A circular mask and UV transparent lens with a focal length of 16.5 cm were used to focus the beam to a 4 mm² spot on the target surface. The laser source was a pulsed KrF excimer laser operating at 248 nm maintained at a 30 ns pulse width with repetition rate of 4 Hz. The laser energy was held at 50 mJ per pulse while the substrate temperature was held at 700 °C. The chamber was evacuated to a base pressure of 10^{−6} Torr and films were grown in a residual background pressure from target ablation of 0.1 mTorr. After the film growth, the samples were cooled down to room temperature in growth pressure at a rate of 10 °C/min.

X-ray diffraction (XRD) and X-ray reflectivity (XRR) analysis (Panalytical X'Pert Pro Diffractometer) was used for phase identification and thickness determination, respectively. Atomic force microscopy (AFM) using a Veeco-DI equipped with a Nanoscope IV Controller and silicon tip from MikroMasch was used in tapping mode to determine surface roughness. High-angle annular dark-field scanning transmission electron microscopy (HAADF-STEM) images and selected area electron diffraction (SAED) were carried out using an aberration corrected FEI Titan 80–300 operated at an accelerating voltage of 300 kV. Raman experiments were carried out using a JYHoriba LabRAM with excitation wavelength 472.95 nm. Wave dispersive spectrometry (WDS) in a scanning electron microscope (JEOL JSM-6490LV

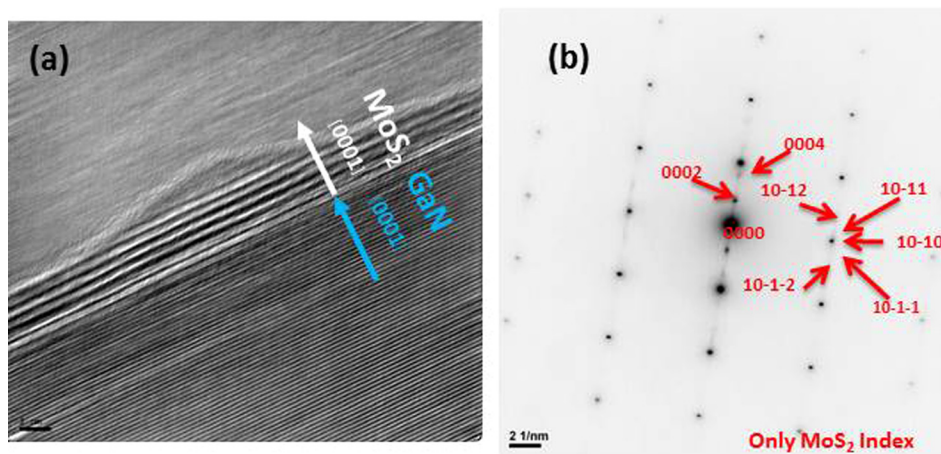


FIG. 1. (a) Cross-sectional TEM image of a MoS₂ sample grown on GaN (0001) demonstrating good stacking of MoS₂ layers with (0001) orientation. (b) Reverse contrast selected area electron diffraction with peaks indexed for MoS₂ showing in-plane quasi-epitaxial relationship $(10\bar{1}0)_{\text{MoS}_2} \parallel (10\bar{1}0)_{\text{GaN}}$.

equipped with Oxford INCAx-Sight) was utilized to determine film composition.

Films with the best crystallinity were obtained from targets with a Mo:S atomic ratio of 1:4. This could lead to sulfur-rich or molybdenum deficient samples leading to p-type doping of the samples as discussed later. Figure 1(a) shows the cross-sectional TEM image of an as-grown MoS₂ thin film on GaN(0001) templated on Al₂O₃(0001). The stacking of MoS₂ (0001) planes on GaN (0001) is clearly visible (See Fig. S1 in supplementary material²⁷ for a large area cross-sectional TEM). Figure 1(b) shows a SAED pattern from the MoS₂ film and GaN substrate with only the MoS₂ film peaks indexed. For both MoS₂ and the GaN substrate, [010] serves as the zone axis, and in both cases, the out-of-plane direction is [001] and the in-plane is [100]. The lack of ring patterns indicates the existence of [001] preferred texture. The in-plane quasi-epitaxial relationship of MoS₂ $(10\bar{1}0) \parallel \text{GaN } (10\bar{1}0)$ can also be distinguished.

XRD patterns in the θ - 2θ mode are attained on films grown on various substrates including Al₂O₃ (0001), GaN (0001), and SiC-6H (0001). Figure 2(a) shows a typical XRD pattern for a 10 nm MoS₂ thin film grown on GaN (0001). The scans were done using the MoS₂ film (0002) peak as the reference. Occurrence of only $(00l)$ peak confirms good out-of-plane texture. To estimate the crystallinity of films, rocking curves around the MoS₂ (0002) peak are measured. The elongation of the rocking curve is seen at different Φ angles indicating that the grown films exhibit

multiple facets. This is discussed in detail in the supplementary information (Figs. S2–S4).²⁷ However, the FWHM of these rocking curves is as low as 0.01°. This indicates a high degree of crystallinity in a given region. A rocking curve on aligned MoS₂ facet on SiC is shown in Fig. 2(b). Similar corrugations were also observed in graphene films when supported on oxide substrates due to the van der Waals interaction coupled with in-plane mismatch strain.²⁸

Raman spectroscopy has been extensively used to characterize MoS₂ films of a few layer thicknesses.^{14,29,30} The E_{2g}¹ mode results from the in-plane vibrations of the two sulfur atoms in opposite directions with respect to the Mo atom, and the A_g¹ mode is a result of the vibration of the S atomic sheets in opposite directions with respect to Mo layer.^{14,29,30} As shown experimentally, when the number of layers decreases, the A_g¹ peak blue shifts as a result of the inter-layer van der Waals interaction in MoS₂, resulting in higher force constants. By contrast, the E_{2g}¹ peak red shifts. This red shift is thought to be due to stacking induced structural changes or long-range Coulombic intra-layer interactions in thicker MoS₂, which may dominate the change in atomic vibration frequency.^{14,30} The difference between the in-plane E_{2g}¹ mode and out-of-plane A_g¹ mode in the Raman spectrum, δ , is representative of the film's thickness with decreasing difference between the peaks corresponding to a decrease in the film thickness.

All of our thin films have a similar Raman signal in terms of peak position, peak height and line shape irrespective of the substrate on which they are grown suggesting that the films only weakly adhere to the diverse substrates by van der Waals forces (Fig. 3(a)). We clearly observe the thickness effect in our samples with the thinnest samples (1 ML) showing a $\delta \approx 20.5 \text{ cm}^{-1}$ and the thickest films showing bulk like behavior with $\delta = 25 \text{ cm}^{-1}$. The thickness of the film is controlled by regulating the number of laser pulses. A growth rate is calculated by x-ray reflectivity measurements and this rate is further confirmed for films of only a few monolayers by TEM and Raman spectroscopy. Raman spectra for one, two, and eight monolayers of MoS₂ are shown in Figure 3(b). In order to demonstrate the uniformity of our samples, Raman measurements are performed on all four corners of a $5 \times 5 \text{ mm}^2$ representative sample. Figure 3(c) shows the Raman spectrum taken at bottom left (BL), top left (TL), top right (TR), and bottom right (BR) on a two mono-layer

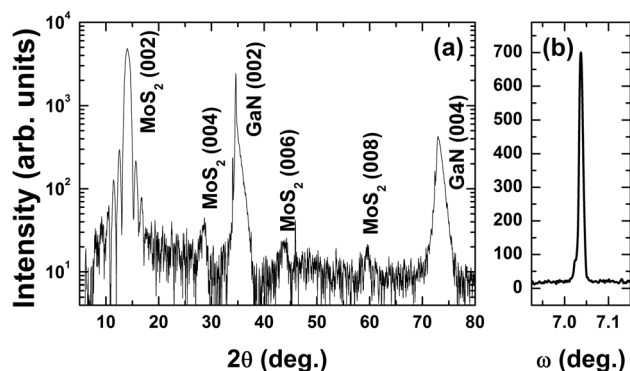


FIG. 2. (a) 2θ XRD pattern of MoS₂ on GaN showing good out of plane texture. (b) Rocking curve of the MoS₂ film on SiC(0001) displaying a FWHM of 0.01°.

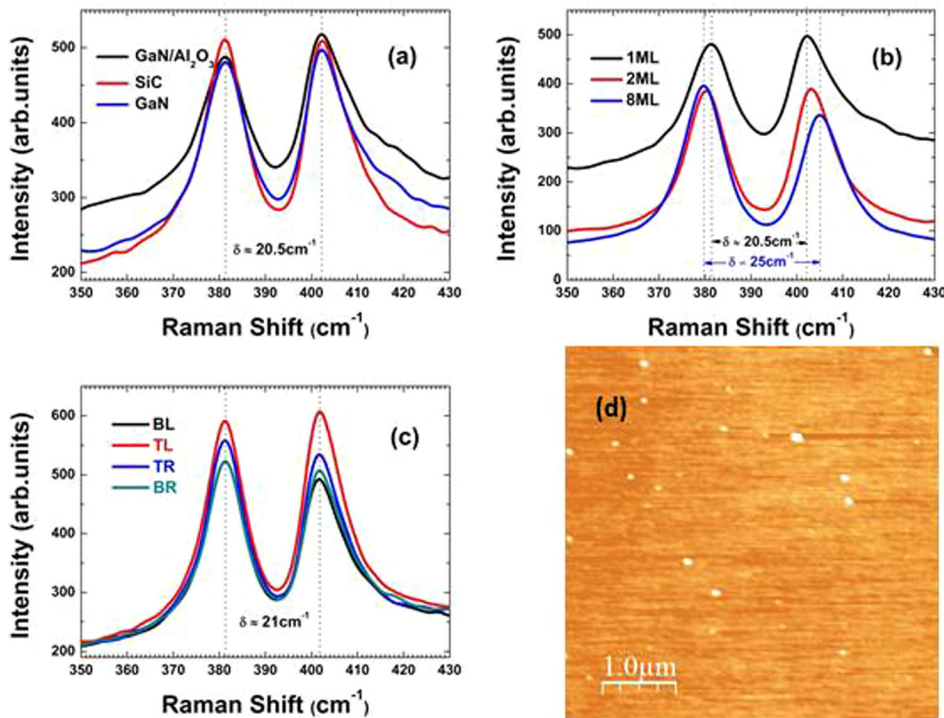


FIG. 3. (a) Raman spectra of a monolayer MoS_2 on $\text{GaN}/\text{Al}_2\text{O}_3$ (0001) (black), SiC-6H (0001) (red) and GaN (0001) (blue); (b) Raman spectra showing the effect of MoS_2 thickness variation, all films were grown on GaN substrate; (c) Raman microprobe measurement displaying curves correspond to the four corner positions, bottom left (BL), top left (TL), top right (TR), and bottom right (BR) of a $5 \times 5 \text{ mm}^2$ two-monolayer thick MoS_2 films grown GaN indicating good uniformity over the area. (d) AFM micrograph exhibiting a RMS roughness of 0.27 nm for the monolayer MoS_2 film on GaN .

MoS_2 film grown on SiC . From the figure, it is clear that the separation between the E_{2g}^1 peak and A_{1g}^1 peaks is constant for the four locations confirming the high degree of thickness uniformity in our sample over a larger area. In addition, the surface topography for the film was measured by AFM. As shown in Fig. 3(d), the surface of the thin MoS_2 film was found to be smooth with a RMS roughness of 0.27 nm. However, as the film thickness increases, RMS roughness increases rapidly, due to particulates that are readily seen on the films.

Electrical characterization was carried out on an 8 nm MoS_2 film on a $\text{GaN}(0001)$ substrate. A schematic

representation of the top gated device is shown in Fig. 4(a) while an optical micrograph is shown in Fig. 4(b). 15 nm thick Al_2O_3 grown by atomic layer deposition (ALD) is used as a gate dielectric. The gate voltage V_G was swept while holding the drain voltage V_D constant and the drain current I_D , and probe potentials (V_1, V_2) were monitored. Fig. 4(c) illustrates the electrical connections for the gated four-probe configuration. Voltage sources were used to apply V_D and to measure the source current I_S and drain current I_D . Voltage monitoring units (VMU) were used to monitor V_1 and V_2 via channel probes and to source V_G . From small signal

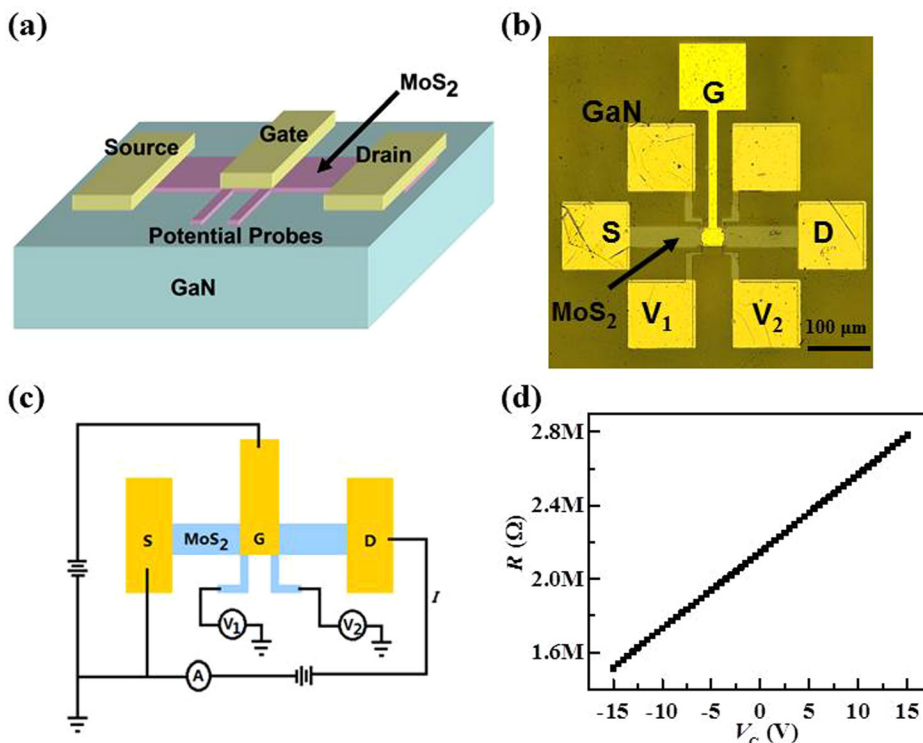


FIG. 4. (a) Schematic of top-gate MoS_2 transistor device geometry. (b) Optical micrograph of the MoS_2 transistor structure showing the GaN substrate, patterned MoS_2 films as the channel, and the source, drain, and channel potential electrodes (Ti 3 nm/Au 50 nm). (c) Circuit schematic for the top-gate four-probe MoS_2 transistor. Channel dimensions are $W = 30 \mu\text{m}$, $L(L1-L2) = 30 \mu\text{m}$. (d) During I_D - V_G sweeps, the source electrode is held at ground and V_D is held constant (2.5 V) as V_G is swept. Current into the source and out of the drain electrode is monitored. The channel potential is measured during V_G sweeping. The close alignment of the edge of top-gate to the potential probes ensures that the potentials monitored at V_1 and V_2 are only of the gated channel region.

resistance measurement, the gated-channel resistance increased by $2X$ as V_G was swept from -15 V to $+15$ V, indicating that the MoS₂ film is p-type (Fig. 4(d)). A resistivity of $1.6 \Omega\text{-cm}$ is found that indicates the presence of reasonably large defect densities. Recently, McDonnell *et al.* showed³¹ that p-type doping of MoS₂ could occur in either S-rich (anti-sites, intercalates or interstitials) or Mo-deficient samples. Given that our ablation target is highly rich in sulfur, we attribute the p-type nature of our films to excess sulfur content induced doping.

To summarize, thin films of MoS₂ were synthesized using pulsed laser deposition on Al₂O₃ (0001), GaN (0001), and SiC-6H (0001) substrates. The as-grown films show high degree of crystallinity and out-of-plane texture. However, no direct epitaxial strain control from the substrate was observed. The as-grown films were also found to be p-doped. Nevertheless, unlike many other growth approaches where only small areas of crystalline material have been synthesized, our work provides a uniform film over the entire substrate. With detailed study of defect formation in the film growth and subsequent growth optimization, PLD could provide a pathway to achieve large area, crystalline, TMD thin films.

This work was supported in part by Army Research Office contract no:W911NF-13-1-0224, Air Force Office of Scientific Research contract no: FA9550-13-1-0114, NSF grant number DMR-1207053 (RM and CC), and the IRICE program at UC Berkeley.

¹A. H. C. Neto, F. Guinea, N. M. R. Peres, K. S. Novoselov, and A. K. Geim, *Rev. Mod. Phys.* **81**, 109 (2009).

²A. K. Geim, *Science* **324**, 1530 (2009).

³K. S. Novoselov, D. Jiang, F. Schedin, T. J. Booth, V. V. Khotkevich, S. V. Morozov, and A. K. Geim, *Proc. Nat. Acad. Sci. USA* **102**, 10451 (2005).

⁴A. A. Balandin, S. Ghosh, W. Bao, I. Calizo, D. Teweldebrhan, F. Miao, and C. N. Lau, *Nano Lett.* **8**, 902 (2008).

⁵A. S. Mayorov, R. V. Gorbachev, S. V. Morozov, L. Britnell, R. Jalil, L. A. Ponomarenko, P. Blake, K. S. Novoselov, K. Watanabe, T. Taniguchi, and A. K. Geim, *Nano Lett.* **11**, 2396 (2011).

⁶Y. Yoon, K. Ganapathi, and S. Salahuddin, *Nano Lett.* **11**, 3768 (2011).

⁷B. Radisavljevic, A. Radenovic, J. Brivio, V. Giacometti, and A. Kis, *Nat. Nanotechnol.* **6**, 147 (2011).

⁸S. Kim, A. Konar, W. Hwang, J. H. Lee, J. Lee, J. Yang, C. Jung, H. Kim, J. Yoo, J. Choi, Y. W. Jin, S. Y. Lee, D. Jena, W. Choi, and K. Kim, *Nat. Commun.* **3**, 1011 (2012).

⁹H. S. R. Matte, A. Gomathi, A. K. Manna, D. J. Late, R. Datta, S. K. Pati, and C. N. R. Rao, *Angew. Chem. Int. Ed.* **49**, 4059 (2010).

¹⁰Z. Zeng, Z. Yin, X. Huang, H. Li, Q. He, G. Lu, F. Boey, and H. Zhang, *Angew. Chem. Int. Ed.* **50**, 11093 (2011).

¹¹G. Eda, H. Yamaguchi, D. Voiry, T. Fujita, M. Chen, and M. Chhowalla, *Nano Lett.* **11**, 5111 (2011).

¹²K. F. Mak, C. Lee, J. Hone, J. Shan, and T. F. Heinz, *Phys. Rev. Lett.* **105**, 136805 (2010).

¹³W. M. R. Divigalpitiya, R. F. Frindt, and S. R. Morrison, *Science* **246**, 369 (1989).

¹⁴C. Lee, H. Yan, L. E. Brus, T. F. Heinz, J. Hone, and S. Ryu, *ACS Nano* **4**, 2695 (2010).

¹⁵A. Splendiani, L. Sun, Y. Zhang, T. Li, J. Kim, C. Y. Chim, G. Galli, and F. Wang, *Nano Lett.* **10**, 1271 (2010).

¹⁶K. G. Zhou, N. N. Mao, H. X. Wang, Y. Peng, and H. L. Zhang, *Angew. Chem. Int. Ed.* **50**, 10839 (2011).

¹⁷Y. Peng, Z. Meng, C. Zhong, J. Lu, W. Yu, Y. Jia, and Y. Qian, *Chem. Lett.* **30**, 772 (2001).

¹⁸C. Altavilla, M. Sarno, and P. Ciambelli, *Chem. Mater.* **23**, 3879 (2011).

¹⁹J. Pütz and M. A. Aegerter, *J. Sol-Gel Sci. Technol.* **19**, 821 (2000).

²⁰Y. Lee, X. Zhang, W. Zhang, M. Chang, C. Lin, K. Chang, Y. Yu, J. T. Wang, C. Chang, L. Li, and T. Lin, *Adv. Mater.* **24**, 2320 (2012).

²¹L. Ma, D. N. Nath, E. W. Lee II, C. H. Lee, M. Yu, A. Arehart, S. Rajan, and Y. Wu, *Appl. Phys. Lett.* **105**, 072105 (2014).

²²S. Helveg, J. V. Lauritsen, E. Lægsgaard, I. Stensgaard, J. K. Nørskov, B. S. Clausen, H. Topsøe, and F. Besenbacher, *Phys. Rev. Lett.* **84**, 951 (2000).

²³J. V. Lauritsen, J. Kibsgaard, S. Helveg, H. Topsøe, B. S. Clausen, E. Lægsgaard, and F. Besenbacher, *Nat. Nanotechnol.* **2**, 53 (2007).

²⁴C. Muratore, J. J. Hu, B. Wang, M. A. Haque, J. E. Bultman, M. L. Jespersen, P. J. Shamberger, M. E. McConney, R. D. Naguy, and A. A. Voievodin, *Appl. Phys. Lett.* **104**, 261604 (2014).

²⁵D. J. Late, P. A. Shaikh, R. Khare, R. V. Kashid, M. Chaudhary, M. A. More, and S. B. Ogale, *ACS Appl. Mater. Interfaces* **6**, 15881 (2014).

²⁶T. A. J. Loh and D. H. C. Chua, *ACS Appl. Mater. Interfaces* **6**, 15966 (2014).

²⁷See supplementary material at <http://dx.doi.org/10.1063/1.4907169> for the experimental details.

²⁸Z. H. Aitken and R. Huang, *J. Appl. Phys.* **107**, 123531 (2010).

²⁹P. A. Bertrand, *Phys. Rev. B* **44**, 5745 (1991).

³⁰H. Li, Q. Zhang, C. C. R. Yap, B. K. Tay, T. H. T. Edwin, A. Olivier, and D. Baillargeat, *Adv. Funct. Mater.* **22**, 1385 (2012).

³¹S. McDonnell, R. Addou, C. Buie, R. M. Wallace, and C. L. Hinkle, *ACS Nano* **8**(3), 2880 (2014).